Structural and functional studies on the extracellular domain of BST2/tetherin in reduced and oxidized conformations

Heidi L. Schubert[a,1], Qianting Zhai[a,1], Virginie Sandrin[a], Debra M. Eckert[a], Mitla Garcia-Maya[b], Louise Saul[b], Wesley I. Sundquist[a,2], Roberto A. Steiner[b,2], and Christopher P. Hill[a,2]

[a]Department of Biochemistry, University of Utah School of Medicine, Salt Lake City, UT 84112-5650; and [b]Randall Division of Cell and Molecular Biophysics, King's College London, New Hunt's House, Guy's Campus, London, SE1 1UL, United Kingdom

Edited* by Stephen C. Harrison, Harvard Medical School, Boston, MA, and approved August 17, 2010 (received for review June 11, 2010)

HIV-1 and other enveloped viruses can be restricted by a host cellular protein called BST2/tetherin that prevents release of budded viruses from the cell surface. Mature BST2 contains a small cytosolic region, a predicted transmembrane helix, and an extracellular domain with a C-terminal GPI anchor. To advance understanding of BST2 function, we have determined a 2.6 Å crystal structure of the extracellular domain of the bacterially expressed recombinant human protein, residues 47–152, under reducing conditions. The structure forms a single long helix that associates as a parallel dimeric coiled coil over its C-terminal two-thirds, while the N-terminal third forms an antiparallel four-helix bundle with another dimer, creating a global tetramer. We also report the 3.45 Å resolution structure of BST2(51-151) prepared by expression as a secreted protein in HEK293T cells. This oxidized construct forms a dimer in the crystal that is superimposable with the reduced protein over the C-terminal two-thirds of the molecule, and its N terminus suggests pronounced flexibility. Hydrodynamic data demonstrated that BST2 formed a stable tetramer under reducing conditions and a dimer when oxidized to form disulfide bonds. A mutation that selectively disrupted the tetramer (L70D) increased protein expression modestly but only reduced antiviral activity by approximately threefold. Our data raise the possibility that BST2 may function as a tetramer at some stage, such as during trafficking, and strongly support a model in which the primary functional state of BST2 is a parallel disulfide-bound coiled coil that displays flexibility toward its N terminus.

coiled coil | crystal structures | HIV | innate immunity | restriction factor

Viral infection can induce a type I interferon response, which in turn stimulates the expression of many genes that encode innate immunity factors (1). One of the upregulated proteins, bone marrow stromal cell antigen 2 (BST2/tetherin/CD317/HM1.24), inhibits the release of HIV-1 and other enveloped viruses from the surface of cells in which it is expressed (2–10). HIV-1 virions retained at the cell surface in the presence of BST2 are fully formed and mature but remain attached to the cell surface by a protease-sensitive linkage (11, 12) that contains BST2 (13, 14). The retained virions can subsequently be internalized and have been visualized in early and late endosomes, and they may ultimately be degraded following fusion with lysosomes (12).

HIV-1 escapes BST2-mediated restriction through the activity of its accessory protein viral protein U (Vpu) (15–17). Most, but not all (18), studies have found that Vpu reduces cell surface levels of BST2, and the two proteins appear to interact through their transmembrane (TM) domains (19–25). Various mechanisms for BST2 surface downregulation have been proposed, including lysosomal degradation, proteasomal degradation, and/or sequestration/retargeting of BST2 to the trans-Golgi network (reviewed in ref. 8). The general importance of BST2 is indicated by the findings that other viruses use different proteins to overcome BST2 restriction, including the Env/glycoproteins of Ebola virus and some strains of SIV and HIV-2, (4, 26, 27), the negative factor (Nef) protein of other SIV strains (24, 28, 29), and the K5 protein of Kaposi's Herpes Sarcoma virus (30, 31).

The mature BST2 protein has an unusual architecture, comprising a small cytosolic domain and a TM helix at the N terminus (residues 22–44), a glycophosphatidylinositol (GPI) anchor at the C-terminal Ser160 residue, and an approximately 105-residues-long disulfide-rich coiled coil structure predicted for the extracellular domain (32–34). This configuration appears central to function, with the leading model being that virions are held at the cell surface by a bridge in which the extracellular domain of one or, more likely, multiple molecules of BST2 spans the gap between plasma membrane and the membrane of the otherwise detached viral particle (13, 14, 34). It has been argued that the GPI modification targets BST2 to cholesterol-rich regions of the plasma membrane (33), which may concentrate the protein at sites of viral budding. However, removal of the GPI anchor reportedly does not release virions from their tethered state (14). Finally, functions for BST2, independent of viral restriction, have also been proposed in trafficking and signaling (33), and in organization of the subapical actin cytoskeleton (35).

It has been proposed that BST2 forms a parallel dimeric coiled coil that is stabilized by C53–C53, C63–C63, and C91–C91 disulfide bonds. This model is supported by nonreducing SDS/PAGE analyses of mutant proteins isolated from the surface of HEK293T cells (32, 34) and by a recent crystal structure of residues 89–147 of the BST2 extracellular domain (36). Both the N-terminal TM helix and the C-terminal GPI can be incorporated into HIV-1 virions, and it has therefore been suggested that BST2 either forms an antiparallel dimer (14) or that it forms a parallel dimer whose tethering orientation is not critical for viral restriction (34). We also note that the importance of BST2 dimerization has been disputed (37). Remarkably, HIV-1 restriction is preserved (at approximately 10% levels) in cells that express an engineered protein that was designed to maintain the overall BST2 architecture but does not conserve the specific amino acid residue identities (34). Finally, the efficiency of BST2-mediated HIV-1 inhibition appears to be concentration-dependent, because virions that contain BST2 can be released under

Author contributions: H.L.S., Q.Z., V.S., D.M.E., M.G.-M., L.S., W.I.S., R.A.S., and C.P.H. designed research; H.L.S., Q.Z., V.S., D.M.E., M.G.-M., L.S., and R.A.S. performed research; H.L.S., Q.Z., V.S., D.M.E., M.G.-M., L.S., W.I.S., R.A.S., and C.P.H. analyzed data; and H.L.S., V.S., D.M.E., W.I.S., R.A.S., and C.P.H. wrote the paper.

The authors declare no conflict of interest.

*This Direct Submission article had a prearranged editor.

Data deposition: The atomic coordinates and structure factors have been deposited in the Protein Data Bank, www.pdb.org [ID codes 3nwh (reduced BST2) and 2xg7 (oxidized BST2)].

[1]H.L.S. and Q.Z. contributed equally to this work.

[2]To whom correspondence may be addressed. E-mail: wes@biochem.utah.edu, roberto.steiner@kcl.ac.uk, or chris@biochem.utah.edu.

This article contains supporting information online at www.pnas.org/lookup/suppl/doi:10.1073/pnas.1008206107/-/DCSupplemental.

conditions of low BST2 expression (34). These considerations emphasize the importance of determining the oligomeric state(s) of BST2. In an effort to understand the mechanistic basis for BST2 activity better, we have determined crystal structures and solution oligomerization states of oxidized and reduced BST2 proteins and tested the restriction activity of a structure-based mutant that cannot switch oligomerization states when reduced.

Results

Reduced BST2 Crystal Structure. We determined a structure of the human BST2 extracellular domain (residues 47-152) produced in *Escherichia coli* and crystallized in the presence of reductant to 2.6 Å resolution and R/R_{free} values of 26.0%/27.8% (Fig. 1 and Table S1). All but a few of the BST2 residues at the termini of the four molecules in the asymmetric unit were visible, although the central regions (residues 92–117) have relatively weak density and high B values.

Subunits are arranged as parallel dimers that splay apart slightly to form an antiparallel 4-helix bundle over the N-terminal 40 residues and generate a 245 Å-long tetramer in the asymmetric unit (Fig. 1*A*). The remaining two-thirds forms a dimeric coiled coil, with residues 118–150 displaying the standard "knobs-into-holes" packing of *a* and *d* heptad repeat residues seen in classical coiled coils (38–40), and residues 92–117 packing more loosely to display some but not all of the *a* and *d* residue knobs-into-holes interactions (Fig. S1). Equivalent packing for the C-terminal two-thirds was reported by Hinz et al. (36).

Although each of the subunits forms one continuous helix that is devoid of sharp turns, the helices do not all superpose closely over their entire length. The two parallel dimers in the asymmetric unit are very similar to each other and superpose with a root mean square deviation of 0.79 Å over all Cα atoms (Fig. 1*B*), but the two subunits within one parallel dimer show an approximately 30° deflection in the vicinity of residue 90, near the tetramer-dimer transition (Fig. 1*C*). This asymmetry results from small differences spread over several residues and may indicate that the BST2 sequence encodes an asymmetric dimeric structure, although we prefer the explanation that the molecule has inherent flexibility.

C53 and C63 are contained within the N-terminal four-helix bundle while C91 is immediately C-terminal to the bundle. All three cysteines are reduced in this structure, whereas biochemical data indicate that BST2 forms disulfide bonds in the oxidizing environment of the cell exterior (34). Residues C53 and C63 are too far from their partners to form disulfide bonds without disrupting packing of the four-helix bundle region. In contrast, neighboring C91 residues could form a disulfide bond without substantial movement of their main chains from the crystal structure. We have built C91 residues with their sulfur atoms separated by 4.7 Å in this structure because the density, which is relatively poor in this region, does not indicate formation of a disulfide.

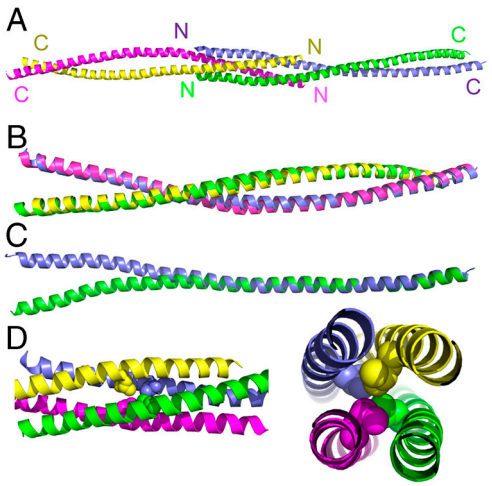

Fig. 1. Structure of reduced BST2(47–152). (*A*) The four molecules in the asymmetric unit. Yellow/magenta and blue/green subunits form parallel dimers. (*B*) Overlap of the two parallel dimers. (*C*) Overlap of the blue and green subunits on residues 90–152. (*D*) Orthogonal views showing the L70 side chain buried at the center of the tetramer.

Oligomeric States in Solution. Equilibrium analytical ultracentrifugation (AUC) was used to determine the association state of recombinant BST2 proteins in solution. This method provides shape-independent estimates of mass and is therefore ideally suited for studies of highly extended assemblies such as BST2. These studies employed slightly longer BST2(47–154) constructs in order to include two tyrosine residues and thereby increase optical absorbance. The AUC data showed that the recombinant protein is a tetramer in solution under the reducing conditions used in crystallization, over an initial concentration range of 0.5–2.0 mg/ml (41.7–166.7 μM). Equilibrium protein distributions could be globally fit to a single species tetramer model (Fig. S2) and also indicated a tetrameric association when the molecular weight was allowed to float (Fig. 2*A*).

To determine if oligomerization was altered by oxidation, purified reduced BST2 was dialyzed for one week against identical buffer that lacked reductant. Mass spectrometry showed that this protein was a fully disulfide-linked dimer (Fig. S3). The protein eluted from a sizing column primarily as a well-defined peak but also included a broad peak at shorter retention times that presumably corresponded to oxidized aggregates. AUC showed that protein from the main peak is dimeric over the concentration range tested (0.5–2.0 mg/ml), either by fitting to a dimer (Fig. S2) or by allowing the molecular weight to float (Fig. 2*B*). These data indicate that BST2 forms a stable tetramer under reducing conditions and converts into a stable dimer upon oxidation.

Oxidized Crystal Structure. To determine the BST2 extracellular domain structure under oxidizing conditions, we expressed secreted BST2(51–151) in HEK293T cells and completed purification and crystallization in the absence of reductant. Crystals of Endo-H treated BST2(51–151) diffracted anisotropically to a maximum resolution of 3.45 Å resolution. This structure, with one dimer in the asymmetric unit, was determined by molecular replacement using residues 89–151 of the reduced structure as a search model. The refined model (R/R_{free} = 26.9%/29.8%) comprises residues 72–151 for one of the two molecules in the asymmetric unit and residues 77–151 for the other molecule. The oxidized and reduced structures overlap closely from residue 90 to the C terminus but diverge toward the N terminus where the reduced protein tetramerizes (Fig. 3). For example, the Cβ–Cβ distance of juxtaposed A88 residues, which occupy an *a* coiled coil position, is 4.2 Å in the oxidized structure and 7.4 Å in the reduced structure. Clear electron density, confirmed by kicked omit maps, is observed for a disulfide bridge linking C91 residues validating the oxidized state of the molecule (Fig. 3). Two sugar moieties extending from N92 and positioned perpendicular to the C91–C91 disulfide could be located in the electron density (Fig. S4). Finally, additional N-terminal residues could be modeled in a helical conformation (Fig. S5), although due to the modest resolution, gaps in the density, and appearance of disorder, we have not included those residues in the deposited model. Thus, the dimeric coiled coil extends into the region that is tetrameric in the reduced structure, and residual density suggests that the coiled coil continues most of the way to the N terminus of this construct, albeit with pronounced flexibility.

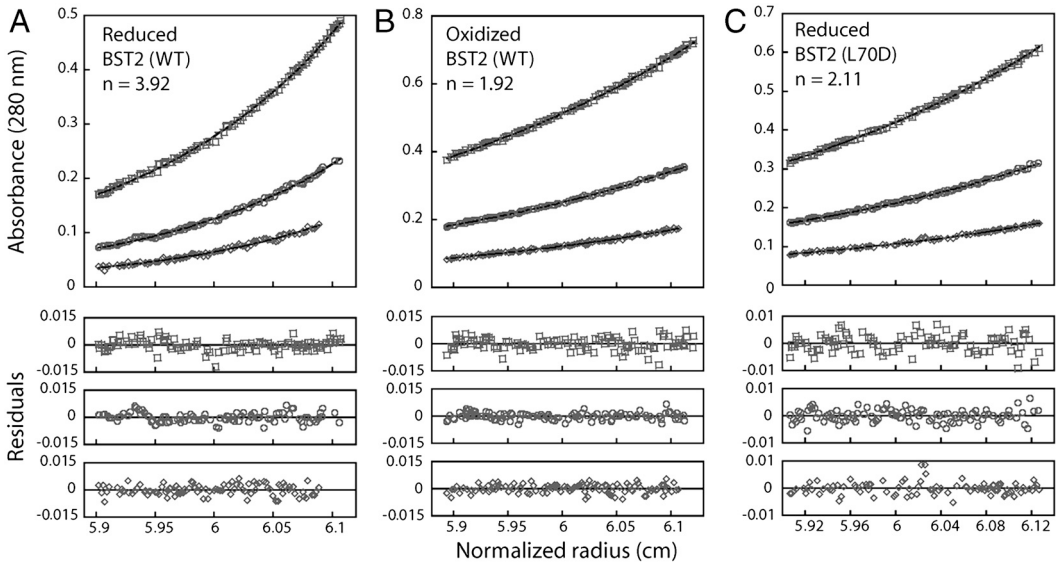

Fig. 2. Analytical equilibrium sedimentation analyses of BST2(47–154) with (*A*) and without (*B*) reductant and of BST2(47–154)L70D with reductant (*C*). Bottom, residual differences between the data and fit. Rotor speeds shown here were 12,000 rpm. Data from two rotor speeds were globally fit to single species models in which the molecular weights were allowed to float. Estimated molecular weights were 50,070 Da for reduced BST2(47–154) ($MW_{obs}/MW_{calc} = 3.92$), 24,497 Da for oxidized BST2(47–154) ($MW_{obs}/MW_{calc} = 1.92$), and 26,908 Da for reduced BST2(47–154)L70D ($MW_{obs}/MW_{calc} = 2.11$).

The Role of the BST2 Tetramer in HIV-1 Restriction. Although the functional importance of many BST2 residues has been tested by mutagenesis (34), the tetramer has not been reported previously. To create a mutant protein that was defective in tetramerization, we mutated Leu70, which lies at the heart of the four-helix bundle (Fig. 1*D*). Mutation to Asp destabilized the tetramer, so that the BST2(147-154)L70D protein remained dimeric, even under reducing conditions (Fig. 2*C* and Fig. S6). Thus, this mutation allowed us to test the restriction activity of a protein that dimerized but did not detectably tetramerize in vitro.

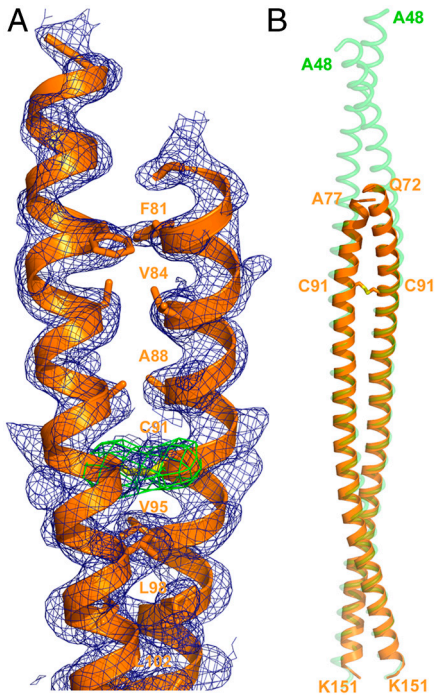

Fig. 3. Structure of oxidized BST2(51–151). (*A*) Electron density for the N-terminal region of oxidized BST2. B-factor sharpening was set at the median B value of refined atoms. $2mF_o$-DF_c map is shown in blue at 1 σ. Maximum-likelihood weighted averaged kick omit map (average size = 100, kick = 0.8 Å) for the C91 disulfide is colored green at 4 σ. Residues at the coiled coil interface are shown. (*B*) Overlap of the reduced (green) and oxidized (orange) structures.

To assay restriction, HEK293T cells (which do not express BST2) were cotransfected with expression constructs for wild-type or mutant BST2 and an HIV-1_{NL4-3} proviral expression construct that lacked Vpu (HIV-$1_{\Delta Vpu}$). BST2(L70D) expression was modestly increased (~1.5-fold) across a series of different concentrations of expression construct (Fig. 4*A*, "Cell" bottom panel). Virus released from cells that expressed wild-type and mutant BST2 was analyzed by (*i*) Western blotting of virion-associated MA and CA proteins in the culture media (Fig. 4*A*, "Virus") and (*ii*) measuring the infectious titers of released virions (Fig. 4*B*). These data showed that both the wild-type and mutant BST2 proteins were effective restriction factors because they reduced the release of infectious viral particles more than 5,000-fold when expressed at high levels. However, the restriction potency of BST2(L70D) was consistently about half that of the wild-type protein, despite higher expression levels (Fig. 4). The strong but attenuated activity of BST2(L70D) indicates that BST2 tetramerization is not essential, although it remains possible that it may contribute to the potency of viral restriction.

Discussion

We have determined crystal structures of the extracellular domain of BST2 under reducing and oxidizing conditions. The C-terminal two-thirds of the structure forms a parallel dimeric coiled coil. The C-terminal third adopts a classical knobs-into-holes packing, while the central third is less well-defined. At the N-terminal third of the protein, the two parallel helices splay apart to form an antiparallel four-helix bundle in the reduced state, but when the protein is oxidized these helices continue, at least initially, as a dimeric coiled coil that is stabilized by a C91–C91 disulfide and probably also by C53–C53 and C63–C63 disulfides. AUC data indicated that the crystal structures recapitulate the predominant solution oligomerization states because the reduced protein forms a stable tetramer but becomes dimeric upon oxidation (Fig. 2). The latter observation is consistent with an earlier study, which concluded that BST2 forms a disulfide-crosslinked dimer on the cell surface (34). Our data therefore indicate that BST2 can tether budded virions to the plasma membrane as a disulfide-linked coiled coil dimer.

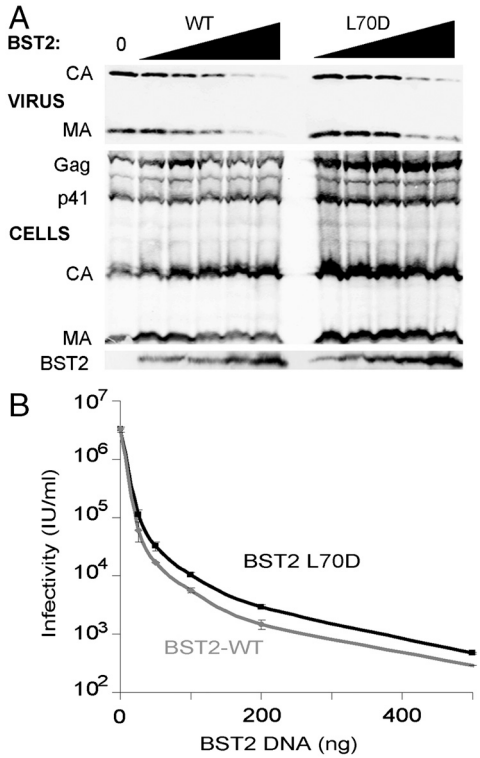

Fig. 4. Inhibition of HIV-1 release and infectivity by BST2 proteins. (*A*) Western blot of samples from 293 T cells that expressed HIV-$1_{\Delta Vpu}$ and either lacked BST2 (lane 1, unrestricted control) or expressed increasing levels of wild-type BST2 (lanes 2–6) or BST2(L70D) (lanes 7–11). Panel 1, levels of virion-associated viral Gag proteins released into the supernatant (VIRUS, anti-CA and anti-MA). Panel 2, intracellular Gag protein levels (CELLS, anti-CA and anti-MA). Panel 3, intracellular BST2 levels (CELLS, anti-BST2). The first lane of Panel 1 contains 25-fold less sample than the other lanes. Quantification showed that, on average, cells transfected with BST2(L70D) expressed 1.4 ± 0.3-fold more protein than those transfected with the wild-type BST2 ($n = 5$, ±s.d.). Nevertheless, cells expressing BST2(L70D) released 2.5 ± 1.3-fold more virion-associated CA and MA protein ($n = 10$, ±s.d.). (*B*) Graph showing HIV-1 titers in the presence of increasing quantities of expression vectors. Wild-type BST2 (light curve), BST2(L70D) (dark curve). Each data point corresponds to a sample analyzed in the Western blots shown in panel *A*. On average, viral titers were 1.9 ± 0.1-fold higher in cells expressing BST2(L70D) mutant (vs. wild-type BST2, $n = 10$, ±s.d.).

While our manuscript was in preparation, a structure of the bacterially expressed C-terminal two-thirds of BST2 (residues 80–147) was reported by Hinz and colleagues (36). This structure showed formation of the C91–C91 disulfide bond, was ordered over residues 89–147, and superimposes closely with our BST2 structures (RMSD = 0.5–0.8 Å over essentially all Cα atoms). This reinforces the impression that the C-terminal two-thirds of the BST2 extracellular domain forms a dimeric coiled coil over both the well packed C-terminal third and over the less regularly associated central third.

Hinz et al. (36) also reported small angle X-ray scattering (SAXS) analysis of dimeric BST2(80–147) and BST2(47–159) proteins. Their data indicate an elongated structure that has a bend at about one third from the N terminus. An attractive possibility is that the N-terminal third of the molecule is flexible, with one specific possibility being that the coiled coil conformation continues toward the N terminus but can hinge about residues approximately 80–90. This apparent flexibility is consistent with (*i*) our finding that residues in this region adopt different conformations in our reduced and oxidized structures (Fig. 3) and in different subunits in the reduced structure (Fig. 1*C*), (*ii*) the appearance of electron density maps for our oxidized BST2(51–151) structure (Fig. 3 and Fig. S5), (*iii*) the protein's protease sensitivity at residue 80 (36), and (*iv*) the retention of tethering activity when an HA tag is introduced following residue 82 (36).

In addition to a hinging motion, it is possible that the N-terminal third of the BST2 extracellular domain has internal flexibility. This would be consistent with the absence of favored buried coiled coil residues in this region of the sequence and our finding that L70D, which corresponds to a buried *d* position in a simple coiled coil model derived from our crystal structures, expresses and purifies like the wild-type sequence and retains activity in a viral restriction assay (Fig. 4). The distribution of cystine residues is compatible with formation of a standard coiled coil throughout the length of the molecule because these residues would occupy *a* (C53), *d* (C63), and *d* (C91) positions in the model extended from the crystal structure. Disulfides can typically be accommodated in these positions, although they are expected to cause some structural perturbation when introduced into an *a* site (41). Just one disulfide is required for stability because constructs lacking any two cystines retain viral restriction activity, albeit with reduced potency (34). The conservation of all three cystines in a region of presumably loose-packed coiled coil is probably not simply due to a requirement for stability because coiled coils can be very stable in the absence of any disulfides. Rather, the cyteine conservation likely reflects a balance between requirements of stability and flexibility for optimal BST2 function.

The model in which BST2 forms a coiled coil from residue 47 to 152 predicts an overall length of 140 Å. This compares with the finding from SAXS measurements that the BST2(47–159) construct has an overall length of 170 Å (36). This 30 Å length difference might be explained by extended conformation(s) for residues 153–159, which are not present in any of the crystal structures plus a few additional residues at the ends of the molecule, which tend to be poorly defined in electron density. Partial unwinding of helices of the N-terminal disulfide-bound portion of the coiled coils is also a possibility.

A number of observations indicate that the N-terminal region of the BST2 extracellular domain is functionally important, including the findings that activity is lost when all disulfide bonds are disrupted (34) or when seven residues within 62–73 are mutated (36). Although we find that the L70D protein retains activity, thereby indicating that formation of a stable reduced tetramer is not essential for viral restriction, the restriction activity is reduced by approximately twofold compared to wild-type, even though expression of the mutant increases slightly. This reduction in potency indicates that L70 contributes to restriction, likely by stabilizing a functional conformation. Indeed, the activity reduction in the L70D mutant approaches the 10-fold loss of activity seen in an "artificial" BST2 molecule that replaces essentially all of the amino acid residues (34). L70D may diminish restriction activity by impacting the conformation or stability of the parallel coiled coil conformation. Alternatively, L70D may diminish activity by inhibiting formation of the reduced BST2 tetramer that, though not absolutely essential for HIV-1 restriction, might contribute to the efficiency of restriction or to some other BST2 function. It is striking that BST2 forms a stable tetramer in solution, indicating that the four-helix bundle is an energetically stable conformation, although we note that isolated coiled coil peptides can adopt nonphysiological association states (42). In principle, tetramerization could occur at several different stages of the BST2 "life cycle." One possibility is that BST2 could become reduced upon localization to a cellular compartment that induces disulfide bond reduction (43, 44), in which case tetramerization could serve as a signal that alters protein trafficking (e.g., promoting BST2 recycling or retention).

Finally, the structure raises the general question, why is BST2 dimeric? Because the leading model is that virions are tethered by the TM helix and GPI anchors binging plasma and viral membranes, one can question why a single isolated subunit is not

sufficient for activity. There are a number of possible explanations, which are not mutually exclusive. Consistent with a report that the GPI anchor is dispensable for restriction (14), one possibility is that virions can be tethered by the two TM helices of a dimer embedding separately in plasma and virion membranes. A second possibility is that dimerization provides a more structured extracellular domain that is better able to fold and resist proteolysis. Third, formation of an extended coiled coil, rather than a more flexible isolated single subunit, may optimally separate the TM helices and GPI anchors, thereby increasing the chance that virions will bud between them and become tethered to the cell. Finally, dimerization may strengthen the tether through avidity effects that result from having two attachments to each membrane. Avidity effects may also explain why higher concentrations of BST2 molecules produce more efficient virion retention (34) because higher order BST2 dimer–dimer interactions could be stabilized in the constrained environment of the cell surface. Although important questions remain regarding the structure of the tether that connects virus and cell, our data indicate that a BST2 parallel coiled coil is likely to be a fundamental component.

Methods

Structure Determination of Reduced BST2. Human BST2(47–152) was expressed in *E.coli*, purified under reducing conditions, and concentrated to 9–16 mg/ml for crystallization (see *SI Text* for details). Crystals grew in sitting drops comprising 2 μl of protein solution and 2 μl of reservoir solution (18% PEG-MME 2K, 0.1 M BisTris pH 7.2, 4 μM TCEP). Crystals were transferred to reservoir solution made up with 30% MPD and plunged into liquid nitrogen. Data were collected from a selenomethione-substituted crystal at SSRL beamline 7.2 and processed with *HKL2000* (45). Eight of the expected twelve Se sites were located using the auto solve option in *Phenix* (46) and phased to 3.0 Å resolution. The model was built using COOT (47) and refined to 2.6 Å with REFMAC5 (48, 49) using translation/libration/screw (TLS) parameters (50) and programs in the CCP4 suite (51). The crystallized construct includes six additional residues (GIDPFT) at the N terminus that are not visible in electron density maps. The following residues lack defined density; molecule A (K47); B (K152); C (K47, K152); D (K47, A48, N49, K151, K152).

Structure Determination of Oxidized BST2. Human BST2(51–151) was expressed in HEK293T cells, purified, and concentrated to approximately 80 mg/ml (Bradford) for crystallization (see *SI Text* for details). MRC crystallization plate sitting drops were set up using a Mosquito crystallization robot by mixing 100 nl of protein solution with an equivalent amount of reservoir. Stacks of platelike crystals grew using a reservoir of 8% PEG8000, 100 mM Tris-HCl pH 8.5 at 18 °C. Crystals were vitrified in crystallization reservoir supplemented with 25% glycerol for data collection at the Diamond Light Source I04 beamline. Data were integrated and scaled using the programs MOSFLM (52) and SCALA (53) of the CCP4 suite. The structure of BST2(51–151) was determined by molecular replacement using PHASER (54) and residues 89–151 of reduced BST2(47–152) as the search model. 20 cycles of rigid-body refinement were followed by 10 cycles of positional refinement using REFMAC5 (48, 49) with the occupancy of C91 residues set to 0.01. $2mF_o$-DF_c and mF_o-DF_c maps indicated the existence of the C91–C91 disulfide and helical density was visible N-terminal to the template. Model building used COOT (47). Final refinement cycles used secondary structure restraints between hydrogen bonded helical N-O atoms. Phenix.refine (55) was used to generate secondary structure restraints and to calculate maximum likelihood averaged kick omit maps (56). The refined model lacks a substantial portion of the N terminus, which could not be reliably built, although residual density is present, particularly in proximity to neighboring molecules in the lattice (Fig. S5).

Analytical Equilibrium Ultracentrifugation. Data were collected at 4 °C in an Optima XL-A centrifuge (Beckman). Reduced BST2(47–154) samples were in a buffer containing 20 mM Tris pH 7.4, 300 mM NaCl, and 4 mM TCEP. Alternatively, BST2(47–154) was oxidized by extensive (1 week) dialysis against the same buffer lacking reductant. Formation of a disulfide-linked dimer upon oxidation was verified by mass spectrometry (Fig. S3). Oxidized and reduced protein samples were centrifuged at 12,000 rpm and 16,000 rpm with initial protein concentrations of 2.1, 1.06, and 0.53 mg/ml (166.7 μM, 83.3 μM, 41.7 μM). Data were globally fit to ideal single species models with fixed or floating molecular masses using the non linear least squares algorithms in the HETEROANALYSIS software (57). Protein partial specific volumes and solvent densities were calculated with the program SEDNTERP (version 1.09) (58).

BST2 Restriction of Virus Release and Infectivity. 293T and HeLa-TZM reporter cells (obtained from Drs. J. C. Kappes and X. Wu through the AIDS Research and Reference Reagent Program, Division of AIDS, NIAID, NIH) were maintained using standard procedures. Wild-type and mutant BST2 proteins were expressed from a pCAG vector under the control of a constitutively active CMV promoter. The HIV-1(ΔVpu) version of the HIV-1 molecular clone NL4-3 has been described previously (12). Virus was produced by calcium phosphate transfection of semiconfluent six well-plates of 293T cells with 1 μg of viral DNA and with increasing quantities of vectors expressing wild-type BST2 WISP10-435 or BST2(L70D) WISP10-436 (0, 25, 50, 100, 200, and 500 ng) or an empty pCAG control vector.

For Western blotting experiments, virus-containing media was harvested 40 h posttransfection. Virions (1 ml) were pelleted through a 20% sucrose cushion at 15,000 × *g*, and the pellet was resuspended in 30 μl 1X SDS/PAGE loading buffer (12 μl loaded/lane). Cells from the same samples were harvested, pelleted, lysed in 60 μl SDS-loading buffer, and boiled for 10 min (6 μl loaded/lane). Levels of virion-associated CA and MA proteins in the culture media (Virus) and cellular Gag-derived and BST2 proteins (Cells) were analyzed by Western blotting using a mouse anti-BST2 (kindly provided by Chugai Pharmaceutical, 1:500 dilutions) or our own rabbit anti-HIV CA and MA antisera (both mixed at 1:1,000). The secondary antibodies were antimouse IgG (goat) polyclonal conjugated to Alexa680 (1:10,000, Invitrogen) and antirabbit IgG (donkey) polyclonal conjugated to IRdye800 (1:10,000, Rockland). Western blots were visualized and quantified using an Odyssey scanner (Li-Cor Biosciences).

Infectious titers were determined from viral supernatants by the numbers of β-galactosidase-positive foci formed on HeLa-TZM indicator cells. Titers provided in Fig. 4*B* show the mean± the range from two independent repetitions of the experiment.

ACKNOWLEDGMENTS. We thank Dr. Stuart J. Neil (King's College London) for contribution in the early stages of the project and Dr. R. Aricescu (University of Oxford) for advice on the mammalian expression system. Portions of this research were carried out at the Stanford Synchrotron Radiation Light Source, (SSRL), a national user facility operated by Stanford University on behalf of the U.S. Department of Energy, Office of Basic Energy Sciences, and at the Diamond Light Source (UK). The SSRL Structural Molecular Biology Program is supported by the Department of Energy, Office of Biological and Environmental Research, and by the National Institutes of Health (NIH), National Center for Research Resources, Biomedical Technology Program, and the National Institute of General Medical Sciences. This work was supported by NIH Grant P50 082545 (W.I.S. and C.P.H.) and a Royal Society Research grant (R.A.S.).

1. Sadler AJ, Williams BR (2008) Interferon-inducible antiviral effectors. *Nat Rev Immunol* 8(7):559–568.
2. Neil SJD, Zang T, Bieniasz PD (2008) Tetherin inhibits retrovirus release and is antagonized by HIV-1 Vpu. *Nature* 451(7177):425–430.
3. Van Damme N, et al. (2008) The interferon-induced protein BST-2 restricts HIV-1 release and is downregulated from the cell surface by the viral Vpu protein. *Cell Host Microbe* 3(4):245–252.
4. Kaletsky RL, Francica JR, Agrawal-Gamse C, Bates P (2009) Tetherin-mediated restriction of filovirus budding is antagonized by the Ebola glycoprotein. *Proc Natl Acad Sci USA* 106(8):2886–2891.
5. Sakuma T, Noda T, Urata S, Kawaoka Y, Yasuda J (2009) Inhibition of Lassa and Marburg virus production by tetherin. *J Virol* 83(5):2382–2385.
6. Jouvenet N, et al. (2009) Broad-spectrum inhibition of retroviral and filoviral particle release by tetherin. *J Virol* 83(4):1837–1844.
7. Groom HC, Yap MW, Galao RP, Neil SJ, Bishop KN (2010) Susceptibility of xenotropic murine leukemia virus-related virus (XMRV) to retroviral restriction factors. *Proc Natl Acad Sci USA* 107(11):5166–5171.
8. Douglas JL, et al. (2010) The great escape: Viral strategies to counter BST-2/tetherin. *PLoS Pathog* 6(5):e1000913.
9. Sauter D, Specht A, Kirchhoff F (2010) Tetherin: Holding on and letting go. *Cell* 141(3):392–398.
10. Arnaud F, et al. (2010) Interplay between ovine bone marrow stromal cell antigen 2/tetherin and endogenous retroviruses. *J Virol* 84(9):4415–4425.
11. Neil SJD, Sandrin V, Sundquist WI, Bieniasz PD (2007) An interferon-[alpha]-induced tethering mechanism inhibits HIV-1 and Ebola virus particle release but is counteracted by the HIV-1 Vpu protein. *Cell Host Microbe* 2(3):193–203.
12. Neil SJD, Eastman SW, Jouvenet N, Bieniasz PD (2006) HIV-1 Vpu promotes release and prevents endocytosis of nascent retrovirus particles from the plasma membrane. *PLoS Pathog* 2(5):e39.

13. Hammonds J, Wang JJ, Yi H, Spearman P (2010) Immunoelectron microscopic evidence for Tetherin/BST2 as the physical bridge between HIV-1 virions and the plasma membrane. *PLoS Pathog* 6(2):e1000749.
14. Fitzpatrick K, et al. (2010) Direct restriction of virus release and incorporation of the interferon-induced protein BST-2 into HIV-1 particles. *PLoS Pathog* 6(3):e1000701.
15. Klimkait T, Strebel K, Hoggan MD, Martin MA, Orenstein JM (1990) The human immunodeficiency virus type 1-specific protein vpu is required for efficient virus maturation and release. *J Virol* 64(2):621–629.
16. Göttlinger HG, Dorfman T, Cohen EA, Haseltine WA (1993) Vpu protein of human immunodeficiency virus type 1 enhances the release of capsids produced by gag gene constructs of widely divergent retroviruses. *Proc Natl Acad Sci USA* 90(14):7381–7385.
17. Varthakavi V, Smith RM, Bour SP, Strebel K, Spearman P (2003) Viral protein U counteracts a human host cell restriction that inhibits HIV-1 particle production. *Proc Natl Acad Sci USA* 100:15154–15159.
18. Miyagi E, Andrew AJ, Kao S, Strebel K (2009) Vpu enhances HIV-1 virus release in the absence of Bst-2 cell surface down-modulation and intracellular depletion. *Proc Natl Acad Sci USA* 106(8):2868–2873.
19. Iwabu Y, et al. (2009) HIV-1 accessory protein Vpu internalizes cell-surface BST-2/tetherin through transmembrane interactions leading to lysosomes. *J Biol Chem* 284(50):35060–35072.
20. Schubert U, et al. (1996) Identification of an ion channel activity of the Vpu transmembrane domain and its involvement in the regulation of virus release from HIV-1-infected cells. *FEBS Lett* 398(1):12–18.
21. McNatt MW, et al. (2009) Species-specific activity of HIV-1 Vpu and positive selection of tetherin transmembrane domain variants. *PLoS Pathog* 5(2):e1000300.
22. Banning C, et al. (2010) A flow cytometry-based FRET assay to identify and analyse protein-protein interactions in living cells. *PLoS One* 5(2):e9344.
23. Rong L, et al. (2009) The transmembrane domain of BST-2 determines its sensitivity to down-modulation by human immunodeficiency virus type 1 Vpu. *J Virol* 83(15): 7536–7546.
24. Jia B, et al. (2009) Species-specific activity of SIV Nef and HIV-1 Vpu in overcoming restriction by tetherin/BST2. *PLoS Pathog* 5(5):e1000429.
25. Lim ES, Malik HS, Emerman M (2010) Ancient adaptive evolution of Tetherin shaped Vpu and Nef functions in human immunodeficiency virus and primate lentiviruses. *J Virol* 84(14):7124–7134.
26. Le Tortorec A, Neil SJ (2009) Antagonism to and intracellular sequestration of human tetherin by the human immunodeficiency virus type 2 envelope glycoprotein. *J Virol* 83(22):11966–11978.
27. Gupta RK, et al. (2009) Simian immunodeficiency virus envelope glycoprotein counteracts tetherin/BST-2/CD317 by intracellular sequestration. *Proc Natl Acad Sci USA* 106 (49):20889–20894.
28. Zhang F, et al. (2009) Nef proteins from simian immunodeficiency viruses are tetherin antagonists. *Cell Host Microbe* 6(1):54–67.
29. Yang SJ, et al. (2010) Anti-tetherin activities in Vpu-expressing primate lentiviruses. *Retrovirology* 7:13.
30. Bartee E, McCormack A, Fruh K (2006) Quantitative membrane proteomics reveals new cellular targets of viral immune modulators. *PLoS Pathog* 2(10):e107.
31. Pardieu C, et al. (2010) The RING-CH ligase K5 antagonizes restriction of KSHV and HIV-1 particle release by mediating ubiquitin-dependent endosomal degradation of tetherin. *PLoS Pathog* 6(4):e1000843.
32. Ohtomo T, et al. (1999) Molecular cloning and characterization of a surface antigen preferentially overexpressed on multiple myeloma cells. *Biochem Bioph Res Co* 258(3):583–591.
33. Kupzig S, et al. (2003) Bst-2/HM1.24 is a raft-associated apical membrane protein with an unusual topology. *Traffic* 4(10):694–709.
34. Perez-Caballero D, et al. (2009) Tetherin inhibits HIV-1 release by directly tethering virions to cells. *Cell* 139(3):499–511.
35. Rollason R, Korolchuk V, Hamilton C, Jepson M, Banting G (2009) A CD317/tetherin-RICH2 complex plays a critical role in the organization of the subapical actin cytoskeleton in polarized epithelial cells. *J Cell Biol* 184(5):721–736.
36. Hinz A, et al. (2010) Structural basis of HIV-1 tethering to membranes by the BST-2/tetherin ectodomain. *Cell Host Microbe* 7(4):314–323.
37. Sakuma T, Sakurai A, Yasuda J (2009) Dimerization of tetherin is not essential for its antiviral activity against Lassa and Marburg viruses. *PLoS One* 4(9):e6934.
38. Crick FH (1953) The packing of α-helices: Simple coiled-coils. *Acta Crystallogr* 6:689–697.
39. O'Shea EK, Klemm JD, Kim PS, Alber T (1991) X-ray structure of the GCN4 leucine zipper, a two-stranded, parallel coiled coil. *Science* 254(5031):539–544.
40. Walshaw J, Woolfson DN (2001) Socket: a program for identifying and analysing coiled-coil motifs within protein structures. *J Mol Biol* 307(5):1427–1450.
41. Zhou NE, Kay CM, Hodges RS (1993) Disulfide bond contribution to protein stability: positional effects of substitution in the hydrophobic core of the two-stranded alpha-helical coiled-coil. *Biochemistry* 32(12):3178–3187.
42. Garcia P, et al. (2006) Molecular insights into the self-assembly mechanism of dystrophia myotonica kinase. *FASEB J* 20(8):1142–1151.
43. Dube M, et al. (2010) Antagonism of tetherin restriction of HIV-1 release by Vpu involves binding and sequestration of the restriction factor in a perinuclear compartment. *PLoS Pathog* 6(4):e1000856 (in eng).
44. Feener EP, Shen WC, Ryser HJ (1990) Cleavage of disulfide bonds in endocytosed macromolecules. A processing not associated with lysosomes or endosomes. *J Biol Chem* 265(31):18780–18785.
45. Otwinowski Z, Minor W (1997) Processing of X-ray diffraction data collected in oscillation mode. *Methods Enzymol* 276:307–326.
46. Adams PD, et al. (2010) PHENIX: A comprehensive Python-based system for macromolecular structure solution. *Acta Crystallogr D* 66(Pt 2):213–221.
47. Emsley P, Cowtan K (2004) Coot: Model-building tools for molecular graphics. *Acta Crystallogr D* 60(Pt 12 Pt 1):2126–2132.
48. Murshudov GN, Vagin AA, Dodson EJ (1997) Refinement of macromolecular structures by the maximum-likelihood method. *Acta Crystallogr D* 53(Pt 3):240–255.
49. Steiner RA, Lebedev AA, Murshudov GN (2003) Fisher's information in maximum-likelihood macromolecular crystallographic refinement. *Acta Crystallogr D* 59(Pt 12): 2114–2124.
50. Painter J, Merritt EA (2006) Optimal description of a protein structure in terms of multiple groups undergoing TLS motion. *Acta Crystallogr D* 62(Pt 4):439–450.
51. CCP4 (1994) The CCP4 suite: Programs for protein crystallography. *Acta Crystallogr D* 50(Pt 5):760–763.
52. Leslie AGW (1992) Recent changes to the MOSFLM package for processing film and image plate data. *Joint CCP4 + ESF-EAMCB Newsletter on Protein Crystallography* No. 26:27–33.
53. Evans P (2006) Scaling and assessment of data quality. *Acta Crystallogr D* 62(Pt 1): 72–82.
54. McCoy AJ, et al. (2007) Phaser crystallographic software. *J Appl Crystallogr* 40(Pt 4): 658–674.
55. Adams PD, et al. (2002) PHENIX: Building new software for automated crystallographic structure determination. *Acta Crystallogr D* 58(Pt 11):1948–1954.
56. Praaenikar J, Afonine PV, Guncar G, Adams PD, Turk D (2009) Averaged kick maps: Less noise, more signal… and probably less bias. *Acta Crystallogr D* 65(Pt 9):921–931.
57. Cole JL (2004) Analysis of heterogeneous interactions. *Methods Enzymol* 384:212–232.
58. Laue T, Shah B, Ridgeway T, Pelletier S (1992) *Computer-aided interpretation of analytical sedimentation data for proteins* (Royal Society of Chemistry, Cambridge, UK), pp 90–125.

Supporting Information

Schubert et al. 10.1073/pnas.1008206107

Supporting Methods

Expression and Purification of Reduced BST2. Human BST2(47–152) was cloned into pET151/D-TOPO (Invitrogen) and expressed in BL21(DE3)RIL cells using the autoinduction technique (1). Ni-NTA affinity chromatography, dialysis against 20 mM Tris, pH 8.0, 100 mM NaCl, 2 mM DTT, and cleavage of the His-tag with TEV protease overnight at room temperature, was followed by Q (Buffer A: 20 mM Tris 8.8, 10 mM NaCl, 1 mM DTT; Buffer B: 20 mM Tris 8.8, 1 M NaCl, 1 mM DTT) and size-exclusion chromatography in 20 mM HEPES pH 7.0, 100 mM NaCl, 2 mM DTT. Protein was concentrated to 9–16 mg/ml for crystallization. Identical procedures were used for BST2(47–154) and selenomethionine-substituted BST2(47–152).

Expression and Purification of Oxidized BST2. Human BST2(51–151) was cloned into a pHLsec vector (a kind gift of Dr. Aricescu, Oxford) between the *AgeI* and *KpnI* cloning sites with a C-terminal $GTKH_6$ tag. After secretion signal cleavage, an EGT tripeptide is left at the N terminus resulting in the final EGT-(BST2 E51–K151)-$GTKH_6$ protein product [BST2(51–151)]. Transient protein expression was performed in HEK293T cells essentially as described (2). To facilitate protein deglycosylation, the *N*-glycosylation inhibitor swainsonine was added at a final concentration of 20 μM during DNA-PEI complex formation (3). Four days after transfection, the supernatant was collected for protein purification under nonreducing conditions. Following overnight binding to a His-Trap column (GE Healthcare), BST2(51–151) was eluted in 50 mM phosphate buffer pH 7.5, 300 mM NaCl with a linear (10–300 mM) imidazole gradient. The protein was then dialyzed against 50 mM Tris-HCl buffer, 50 mM NaCl with pH adjusted to 5.5 with a 1 M sodium citrate solution prior to overnight deglycosylation at 37 °C with Endoglycosidase-H (New England Biosciences) according to the manufacturer's instructions. Deglycosylated BST2(51–151) was further purified by size-exclusion chromatography on a S200 16/60 column (GE Healthcare) in 50 mM Tris-HCl pH 7.5, 100 mM NaCl buffer.

1. Studier FW (2005) Protein production by auto-induction in high density shaking cultures. *Protein Expres Purif* 41(1):207–234.
2. Aricescu AR, Lu W, & Jones EY (2006) A time- and cost-efficient system for high-level protein production in mammalian cells. *Acta Crystallogr D* 62(Pt 10):1243–1250.
3. Chang VT et al. (2007) Glycoprotein structural genomics: Solving the glycosylation problem. *Structure* 15(3):267–273.

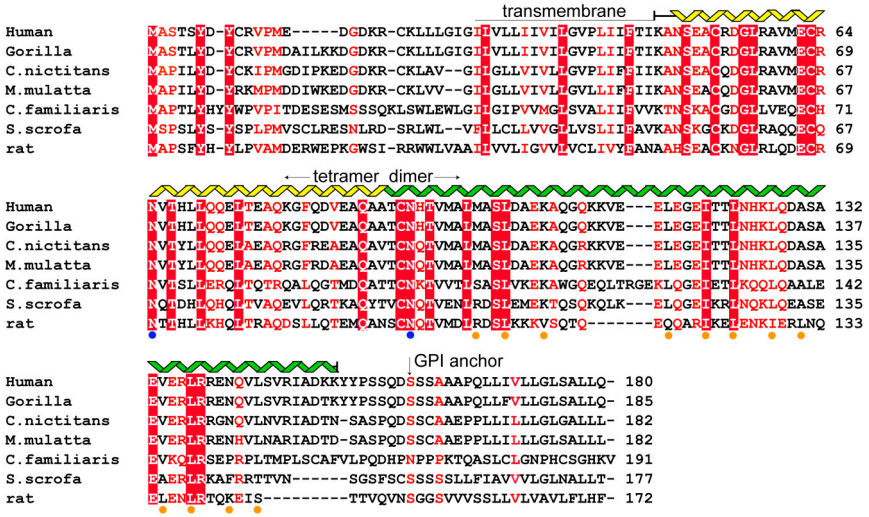

Fig. S1. Sequence alignment with knobs and holes analysis. An alignment of representative sequences with secondary structure observed in the reduced structure shown above. The mature human protein is truncated at Ser160, the site of GPI anchor attachment. The glycosylation sites, Asn65 and Asn92, are indicated with blue dots and are solvent exposed in the crystal structures. Residues that display *a* or *d* knobs into holes packing, as defined by the program SOCKET (1), are indicated with orange dots. Residues that are invariant in this alignment are highlighted in red boxes, and residues that are highly conserved are shown in red.

1. Walshaw J & Woolfson DN (2001) Socket: A program for identifying and analysing coiled-coil motifs within protein structures. *J Mol Biol* 307(5):1427–1450.

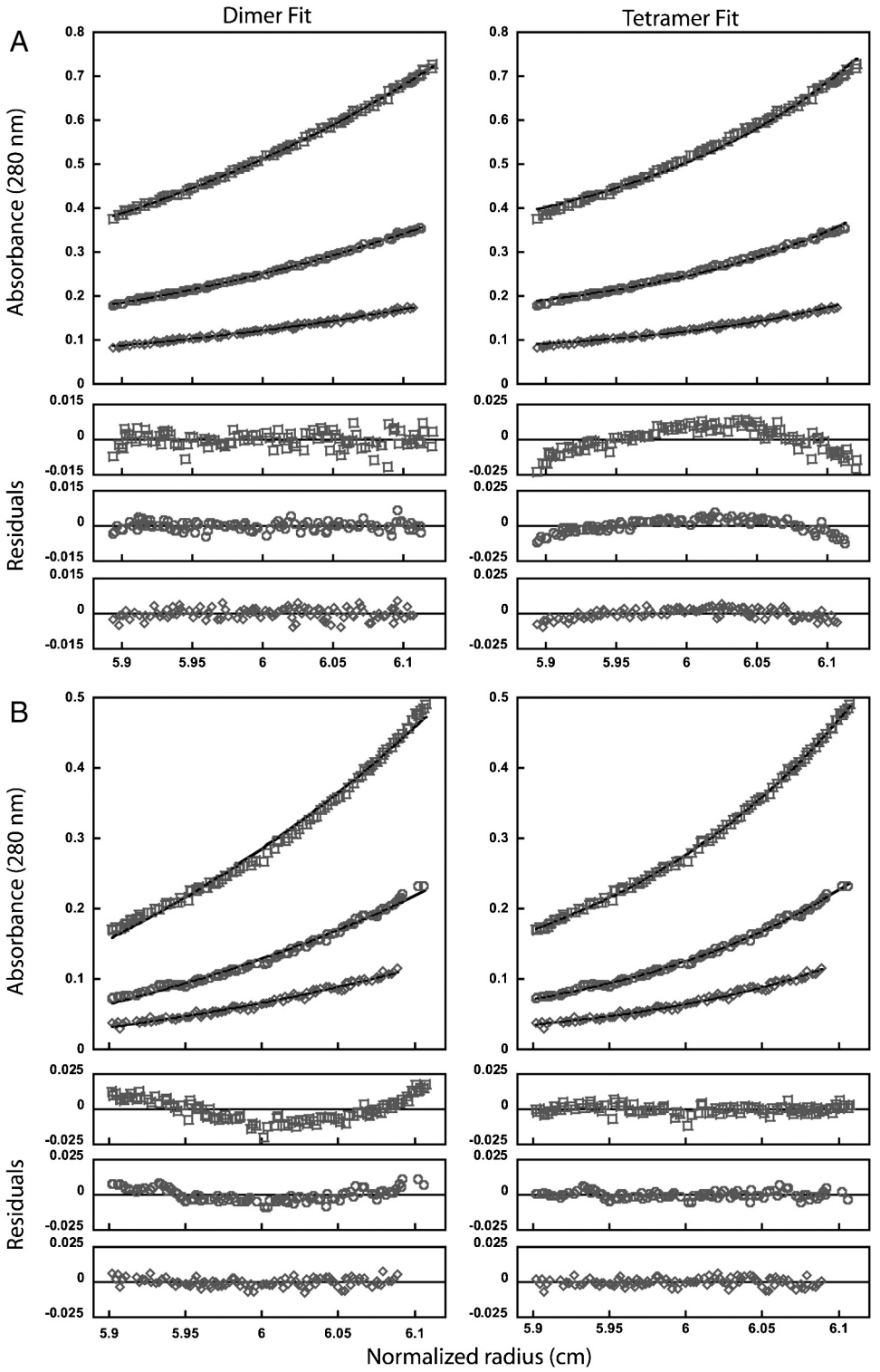

Fig. S2. Analytical equilibrium ultracentrifugation analyses of BST2(47–154). Equilibrium distributions without (*A*) and with (*B*) reductant (4 mM TCEP). Residual differences between the data and the fits are shown below. Rotor speeds were 12,000 rpm in these experiments. Data sets were also collected at 16,000 rpm. Data were collected at three concentrations and were globally fit to single species models in which the molecular weights were fixed to either a tetramer (left panel; 51,100 Da) or dimer (right panel, 25,550 Da). Note that the reduced BST2 protein is well fit by the tetramer model and the oxidized protein is well fit by the dimer model.

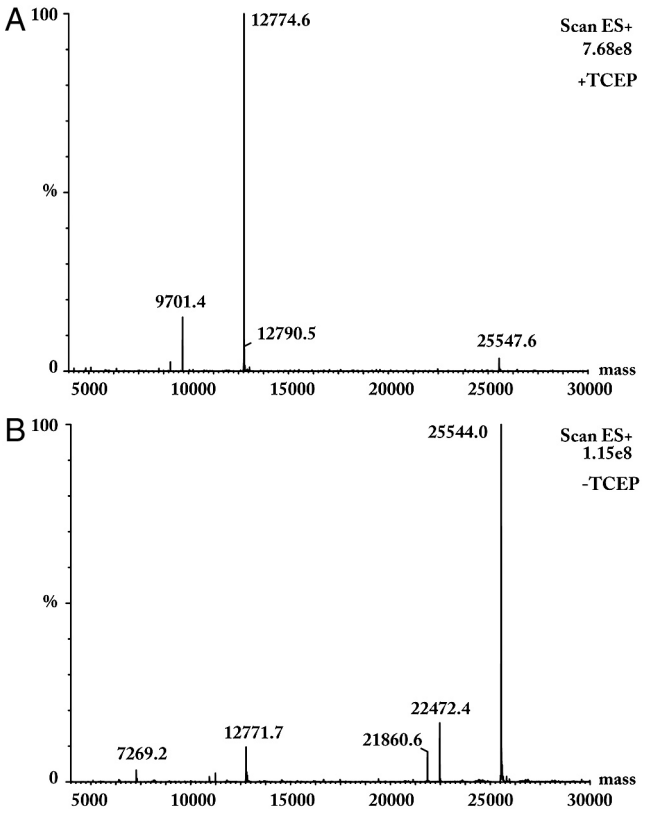

Fig. S3. Mass spectrometry of reduced and oxidized BST2(47–154). (*A*) Reduced and (*B*) oxidized BST2(47–154) were desalted for electrospray ionization mass spectrometry using a C18 Ziptip (Millipore) and analyzed on a Quattro-II mass spectrometer (Micromass, Inc.). Data were acquired with a cone voltage of 50 eV, a spray voltage of 2.8 kV, and scanning from 800 to 1,400 m/z in 4 s. Spectra were combined, and the multiply charged molecular ions were deconvoluted into a molecular-mass spectrum by using MaxEnt software (Micromass, Inc.). The mass of the reduced species corresponded to a BST2(47–154) monomer (MW_{obs} = 12,774.6 g/mol, MW_{calc} = 12,775.4 g/mol), indicating no disulfide formation in the presence of reductant. In contrast, the majority of BST2(47–154) formed a disulfide crosslinked dimer in the absence of TCEP (MW_{obs} = 25,544.0 g/mol, MW_{calc} = 25544.8 g/mol, assuming formation of three disulfide bonds).

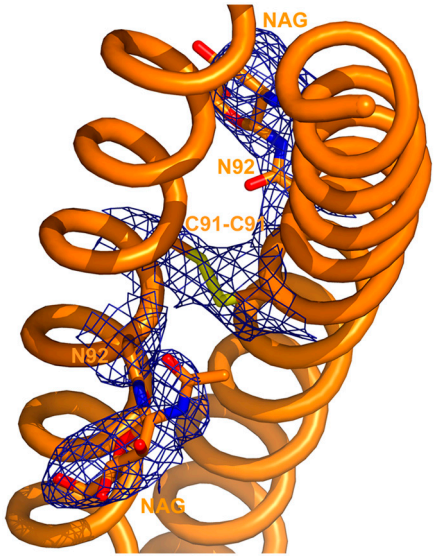

Fig. S4. Density showing glycosylation of N92 in BST2(51–151) expressed in HEK293T cells. $2mF_o$-DF_c electron density (1.0σ, blue) indicates the position of discernible sugar moieties extending from N92 residues after Endo-H treatment. N-acetylglucosamine (NAG) residues are approximately perpendicular to the C91–C91 disulfide bond.

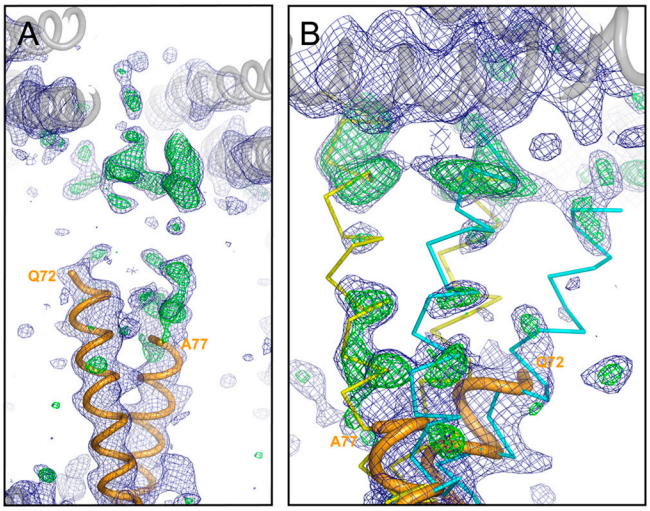

Fig. S5. Residual electron density at the N terminus of oxidized BST2(51–151). (*A*) Density in the $2mF_o$-DF_c (blue, 1.0 σ) and mF_o-DF_c (green, 3.0 σ) maps is visible at the N terminus of BST2(51–151) (orange). It is mostly evident in proximity to symmetry related molecules (gray). (*B*) Residual density suggests the possibility of alternative helical conformation for the N-terminus, which we have tentatively modeled in this figure. Flexibility at the N terminus could generate alternative coiled-coil dimers shown here in cyan and yellow, respectively.

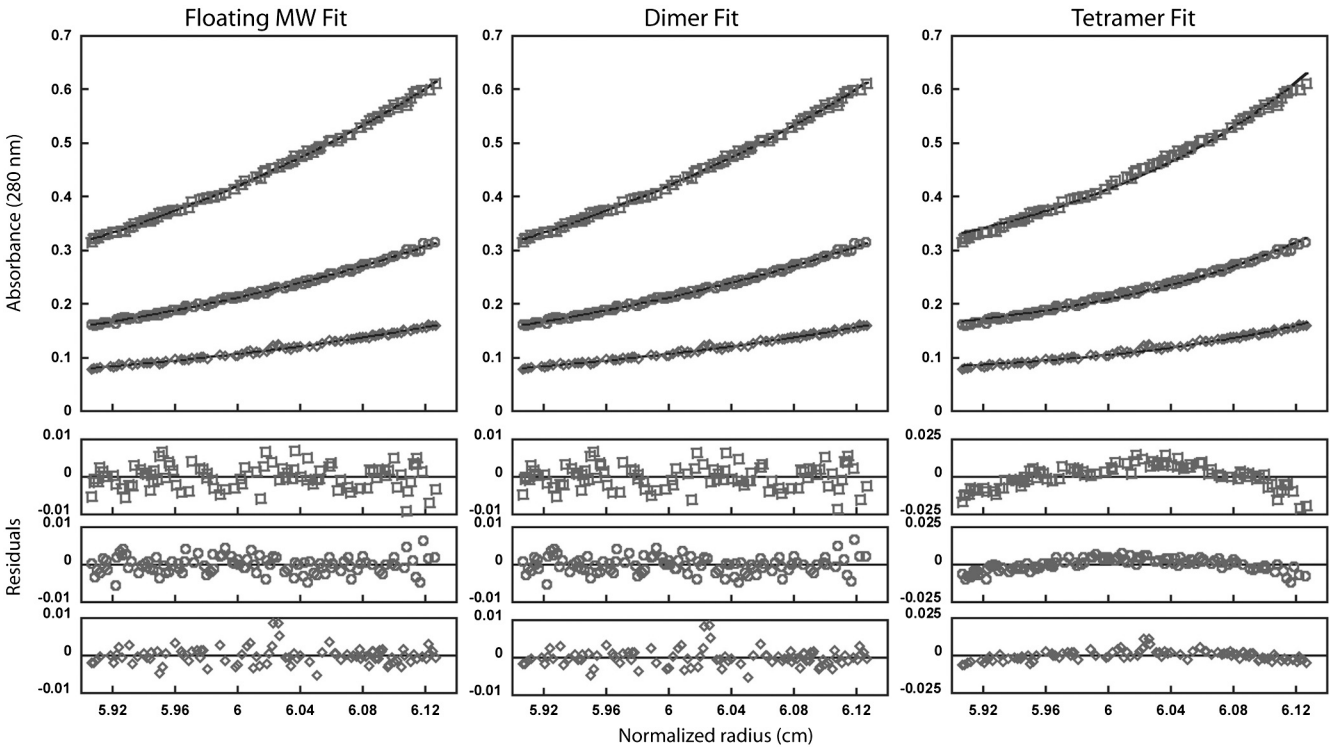

Fig. S6. Analytical equilibrium ultracentrifugation analyses of wt BST2(47–154)L70D. Equilibrium sedimentation distributions of BST2(47–154)L70D with reductant (4 mM TCEP). Corresponding residual differences are shown below. Rotor speeds for the data shown here were 12,000 rpm. Data sets were also collected at 16,000 rpm. Data were collected at three concentrations, and all of the data were globally fit to single species models in which the molecular weight was allowed to float (left panel; $MW_{obs} = 26{,}908$ Da), fixed as a dimer (middle panel; 25,554 Da) and fixed as a tetramer (right panel; 51,108 Da). Note that the reduced BST2(47–154) L70D protein is well fit by the dimer model.

Table S1. Data collection and crystallographic refinement statistics

Data set	Reduced BST2(47-152)	Oxidized BST2(51-151)
PDB code	3nwh	2xg7
Space group	$P2_1$	$P2_12_12_1$
Cell dimensions (Å,°)	$a = 26.6$	$a = 28.86$
	$b = 59.6$	$b = 91.86$
	$c = 159.5$	$c = 146.96$
	$\beta = 91.6$	
Solvent content (%)	57	70
Resolution (Å)	50.00-2.60 (2.69-2.60)	38.95-3.45 (3.64-3.45)
Completeness (%)	97.5 (93.2)	99.4 (97.6)
$I/\sigma(I)$	17.2 (4.0)	8.9 (2.5)
Multiplicity	3.6 (3.3)	6.8 (6.5)
R_{sym} (%) *	5.8 (26.9)	11.3 (70.9)
# Unique reflections	15,096	5,576
Wilson B (Å^2)	46.9	133.4
R factor (%)	26.0	26.9
R_{free} (%) †	28.7	29.8
# of protein atoms	3,266	1,209
# water molecules	18	0
# sugar molecules	-	2
$\langle B \rangle$(Å^2)		
protein atoms	16.4	126.6
water molecules	37.4	-
sugar molecules		181.5
RMSD from ideality		
Bonds (Å)	0.018	0.012
Angles (°)	1.64	1.38
Phi/Psi angles:		
Favored (%)	98	98.04
Allowed (%)	2.0	1.96
Disallowed (%)	0.0	0.0

Values in parentheses are for the highest-resolution shell.

*$R_{sym} = \sum |I - \langle I \rangle| / \sum I$, where $\langle I \rangle$ is the average intensity from multiple observations of equivalent reflections.

†$R_{factor} = 100 \times \sum ||F_o| - |F_c|| / \sum |F_o|$. R_{free} is the R_{factor} computed from the 7.6% of reflections in the case of 3nwh and 4.5% in the case of 2xg7 that were chosen randomly and excluded from the refinement calculations.